PLOS ONE

RESEARCH ARTICLE

Comparison of phase-resolved functional lung (PREFUL) MRI derived perfusion and ventilation parameters at 1.5T and 3T in healthy volunteers

Julian Glandorf[1,2], Filip Klimeš[1,2], Andreas Voskrebenzev[1,2], Marcel Gutberlet[1,2], Lea Behrendt[1,2], Cristian Crisosto[1,2], Frank Wacker[1,2], Pierluigi Ciet[3], Jim M. Wild[4], Jens Vogel-Claussen[1,2]*

1 Institute for Diagnostic and Interventional Radiology, Hannover Medical School, Hannover, Germany, **2** Biomedical Research in Endstage and Obstructive Lung Disease Hannover (BREATH), Member of the German Centre for Lung Research (DZL), Hannover, Germany, **3** Department of Radiology and Nuclear Medicine, Erasmus University Medical Center Rotterdam, Rotterdam, The Netherlands, **4** Department of Infection, Immunity and Cardiovascular Disease, University of Sheffield, Sheffield, United Kingdom

* vogel-claussen.jens@mh-hannover.de

Citation: Glandorf J, Klimeš F, Voskrebenzev A, Gutberlet M, Behrendt L, Crisosto C, et al. (2020) Comparison of phase-resolved functional lung (PREFUL) MRI derived perfusion and ventilation parameters at 1.5T and 3T in healthy volunteers. PLoS ONE 15(12): e0244638. https://doi.org/10.1371/journal.pone.0244638

Editor: Pascal A. T. Baltzer, Medical University of Vienna, AUSTRIA

Received: October 1, 2020

Accepted: December 15, 2020

Published: December 30, 2020

Data Availability Statement: All relevant data are within the manuscript and its Supporting Information files.

Funding: The work was funded by the German Center for Lung Research (DZL) and by the Cystic Fibrosis Foundation (CFF). The funders had no role in study design, data collection and analysis, decision to publish, or preparation of the manuscript.

Abstract

Purpose

The purpose of this study is to evaluate the influence of different field strengths on perfusion and ventilation parameters, SNR and CNR derived by PREFUL MRI using predefined sequence parameters.

Methods

Data sets of free breathing 2d FLASH lung MRI were acquired from 15 healthy subjects at 1.5T and 3T (Magnetom Avanto and Skyra, Siemens Healthcare, Erlangen, Germany) with a maximum period of 3 days in between. The processed functional parameters regional ventilation (RVent), perfusion (Q), quantified perfusion (Q_{Quant}), perfusion defect percentage (QDP), ventilation defect percentage (VDP) and ventilation-perfusion match (VQM) were compared for systematic differences. Signal- and contrast-to-noise ratio (SNR and CNR) of both acquisitions were analyzed.

Results

RVent, Q, VDP, SNR and CNR presented no significant differences between 1.5T and 3T. Q_{Quant} (1.5T vs. 3T, $P = 0.04$), and QDP (1.5T vs. 3T, $P \leq 0.01$) decreased significantly at 3T. Consequently, VQM increased significantly (1.5T vs. 3T, $P \leq 0.01$). Skewness and kurtosis of the Q-values increased significantly at 3T ($P \leq 0.01$). The mean Sørensen-Dice coefficients between both series were 0.91 for QDP and 0.94 for VDP. The Bland-Altman analysis of both series showed mean differences of 4.29% for QDP, 1.23% for VDP and -5.15% for VQM. Using the above-mentioned parameters for three-day repeatability at two different scanners and field strengths, the retrospective power calculation showed, that a

Competing interests: The authors have declared that no competing interests exist.

sample size of 15 can detect differences of 3.7% for QDP, of 2.9% for VDP and differences of 2.6% for VQM.

Conclusion

Significant differences in QDP may be related to field inhomogeneities, which is expressed by increasing skewness and kurtosis at 3T. Q_{Quant} reveals only poor reproducibility between 1.5T and 3T. RVent, Q, VDP, SNR and CNR were not altered significantly at the used sequence parameters. Healthy participants with minimal defects present high spatial agreement of QDP and VDP.

Introduction

The global impact of pulmonary diseases like chronic obstructive pulmonary disease (COPD) and asthma on approximately 400 million people clarifies the urgent need for sensitive methods for early detection, disease monitoring and lung function testing [1, 2]. Functional lung imaging offers promising possibilities, but most of the existing techniques are based on contrast enhancement, additional expensive technical equipment or ionizing radiation [3–6]. Some patient groups are unable to undergo certain techniques based on contrast enhancement or spirometry due to potential allergic reactions or the inability of active participation [7–9]. The pursuit of modern MRI techniques for functional lung proton imaging on a regional scale has led to the development of functional free breathing methods of 1H MRI such as phase resolved functional lung (PREFUL) MRI and similar techniques based on Fourier decomposition (FD) [10–12]. These techniques have already proven their ability to provide information on different functional parameters such as ventilation and perfusion in various diseases and can be used for follow up examinations [13–18]. The radiation free examination during free breathing without the need of contrast enhancement makes PREFUL a valuable method for the majority of patients with chronic lung diseases.

In order to establish the reliability of the method for pulmonary disease monitoring, the comparability of the determined functional parameters has to be evaluated across vendor platforms and field strengths. A previous work already demonstrated the robustness of regional ventilation and unquantified perfusion parameters against T1 shortening by gadolinium-based contrast agents (GBCAs) [19]. Another potential influence on functional parameters could be due to the use of different field strengths and their corresponding sequence parameters. Increasing numbers of 3T systems enter the market, because of the potential increase of signal-to-noise ratio (SNR) and contrast-to-noise ratio (CNR) for most organs when compared to 1.5T [20, 21]. In particular lung imaging could benefit from higher SNR as only low intrinsic signal is available [22]. On the other side, the known susceptibility artifacts caused by multiple air-tissue interfaces may be pronounced and further reduce $T2^*$ relaxation time [21, 23] thus potentially degrading SNR. Therefore, the effects of higher field strengths on functional lung parameters need to be examined to guarantee reproducibility between different scanners and scan sites. Bauman et al. recently analyzed the impact of higher magnetic field strength on SNR, CNR and relative functional parameters derived by matrix pencil decomposition using steady state free precession and a transient state spoiled gradient echo sequence [24]. The purpose of this study is to evaluate the influence of different field strengths on SNR, CNR and the functional parameters derived by PREFUL MRI in a cohort of healthy participants using a commercially available spoiled gradient echo fast low angle shot (FLASH) sequence.

Methods

Participants

The study was approved by the local ethics committee "Ethikkommission" of the "Medizinische Hochschule Hannover" (Study No. 7740_BO_S_2018). Written informed consent was obtained from all participants. Data sets of 16 healthy subjects were acquired and processed. An unequal field of view was used for 1 female participant, who was then excluded due to incomparability of the resulting SNR. The volunteers needed to be 18 to 60 years of age. Exclusion criteria were general inabilities to undergo MRI (e.g. due to claustrophobia, paramagnetic implants, pregnancy). Participants that had a recent (< 1 month) history of lung disease, a chronic lung disease or a known congenital lung disease were excluded.

Imaging technique

All subjects were examined at 1.5T and 3T scanners (Magnetom Avanto and Skyra, Siemens Healthcare, Erlangen, Germany) with a maximum period of 3 days in between exams. The PREFUL MRI examinations were performed using a spoiled gradient echo FLASH sequence with the parameters shown in Table 1. TR and TE were minimized in regards to scan time reduction and the MR signal was maximized using the Ernst angle.

Parallel imaging with GRAPPA with acceleration factor 2 was performed for both acquisitions. All participants were scanned in head first supine position. At 1.5T, 250 images of a single coronal slice at the level of the carina were acquired in ~48 s during free breathing. At 3T, 500 images of the same location were acquired in ~58 s. All images were interpolated to the final in-plane resolution of 256 x 256 pixels prior to reconstruction. The non-uniform intensity profiles of the applied receiver coils were corrected using the sensitivity profiles of the surface and body coil before PREFUL analysis.

Postprocessing

To achieve full saturation and to ensure a steady-state of the stationary tissue, the first 20 images of every PREFUL data set were discarded. All data sets were registered using advanced normalization tools (ANTs) for linear and diffeomorphic image registration with a previously described group oriented registration scheme (GOREG) to achieve a uniform respiratory position for each PREFUL acquisition [25, 26]. In addition, registration between the corresponding 1.5T and 3T series was performed for voxel-wise comparison (see Fig 1). To measure the success of co-registration between 1.5T and 3T, the structural similarity index (SSIM) was calculated [27]. Image guided filtering was applied to all images of every data set using an edge-preserving filter [28].

Each data set was segmented by individual thresholds with the aim to include the vast majority of the lung parenchyma and to exclude large central vessels up to the segmental level.

Table 1. Sequence parameters at 1.5T and 3T.

Sequence Parameter	1.5 Tesla	3 Tesla
Field of view	50 x 50 cm^2	50 x 50 cm^2
Matrix-size	128 x 128	128 x 128
Slice thickness	15 mm	15 mm
Echo time	0.82 ms	0.74 ms
Repetition time	3 ms	1.83 ms
Flip angle	5˚	4˚
Pixel bandwidth	1500 Hz/pixel	1500 Hz/pixel

https://doi.org/10.1371/journal.pone.0244638.t001

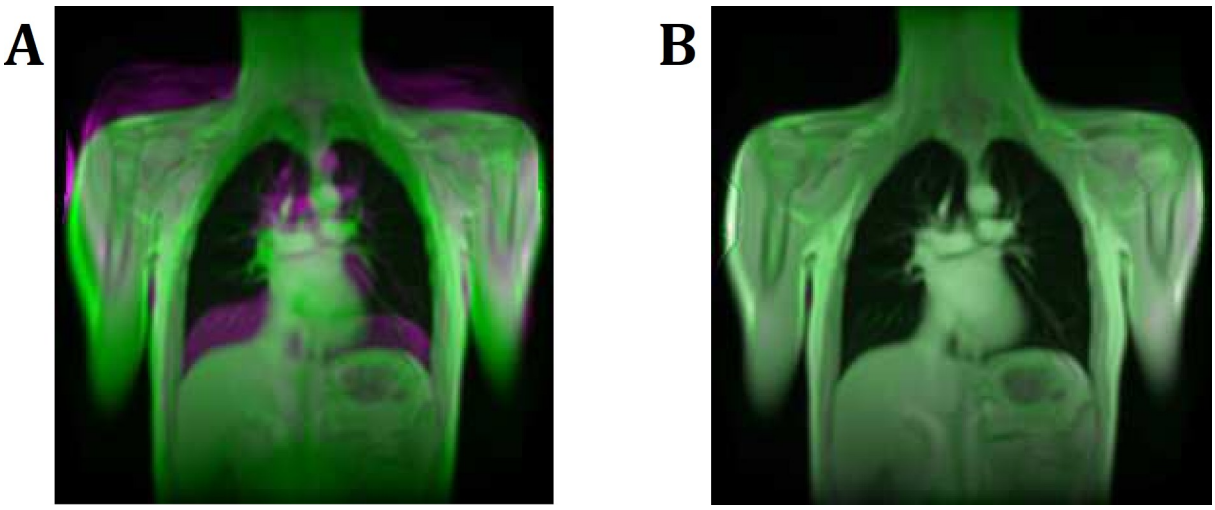

Fig 1. Registration of the 1.5T to the 3T series. Registration between the corresponding 1.5T and 3T series was performed to achieve voxel wise comparability. **A:** Overlay of 1.5T and 3T images before registration. **B:** Overlay image of 1.5T and 3T images after successful registration. Note the increasing structural similarity index (SSIM) of 0.15 before to 0.56 after the registration, which is indicating a successful registration step.

https://doi.org/10.1371/journal.pone.0244638.g001

If needed, the segmentations were optimized by manual corrections of insufficiently segmented structures.

Image outliers due to motion were excluded by removing images outside the intersection of the 1.5T and 3T diaphragm tracking curves. For this, the 3T diaphragm tracking curve was translated onto the 1.5T diaphragm tracking curve by matching the median values of each time series. Furthermore, the total acquisition time of both series was equalized by truncating the 3T time-series (see Fig 2).

PREFUL ventilation analysis

A low-pass filter at 0.8 Hz was used to remove perfusion effects from the registered images and to calculate ventilation-weighted images. The images were sorted according to their respiratory phase based on the averaged signal amplitude of a region of interest (ROI) positioned at the lung-diaphragm. Subsequently, the sorted images were interpolated to a uniform time grid. Finally, ventilation including phase information was calculated [12]. Regional ventilation (RVent) was used to quantify ventilation according to Klimeš et al. [29]:

$$\mathrm{RVent} = \left(\frac{S_{\mathrm{Mid}}}{S_{\mathrm{Insp}}}\right) - \left(\frac{S_{\mathrm{Mid}}}{S_{\mathrm{Exp}}}\right) \quad (1)$$

S_{Exp} and S_{Insp} represent the averaged signals of the end-expiratory and end-inspiratory images. S_{Mid} represents the mean signal of the images in intermediate lung inflation level, which is also used as the reference volume during registration. Ventilation-weighted maps generated at 1.5T and 3T are displayed in Fig 3.

PREFUL perfusion analysis

A high pass filter at 0.75 Hz was applied to the registered images in order to exclude signal changes due to respiration. Similarly to ventilation analysis, the averaged signal of a manually segmented ROI at the aorta was fitted to a piecewise sine function to estimate the cardiac

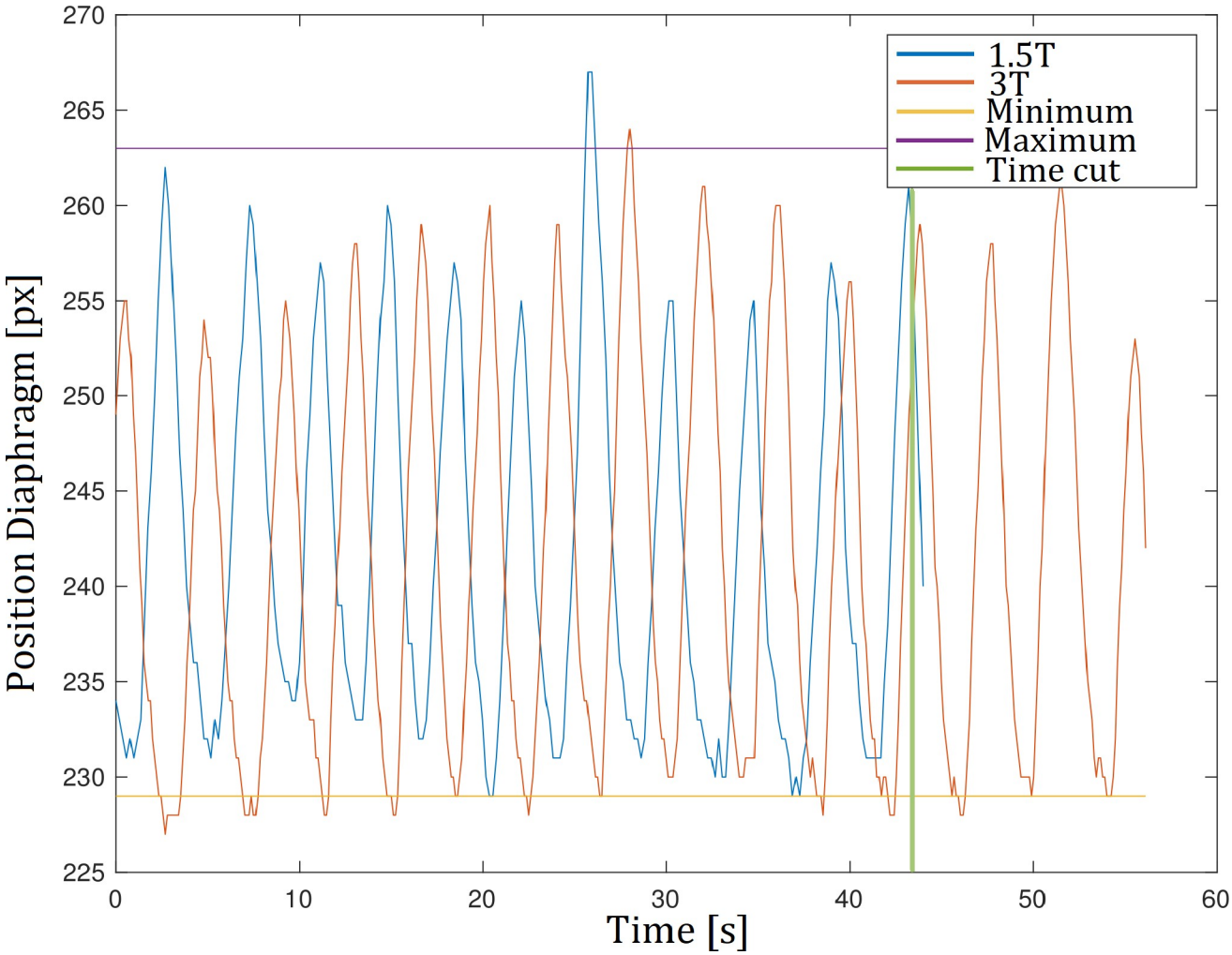

Fig 2. Diaphragm tracking. Respiratory outliers outside the maximum or minimum respiratory level were excluded by removing images outside the intersection of the diaphragm tracking curves of the 1.5T and 3T series. Furthermore, the acquisition time of both series was equalized by truncating the 3T series.

https://doi.org/10.1371/journal.pone.0244638.g002

phase of each time point. Phase information was calculated by sorting the images according to their phase and by interpolating them to an equidistant time grid [12]. Perfusion (Q) was

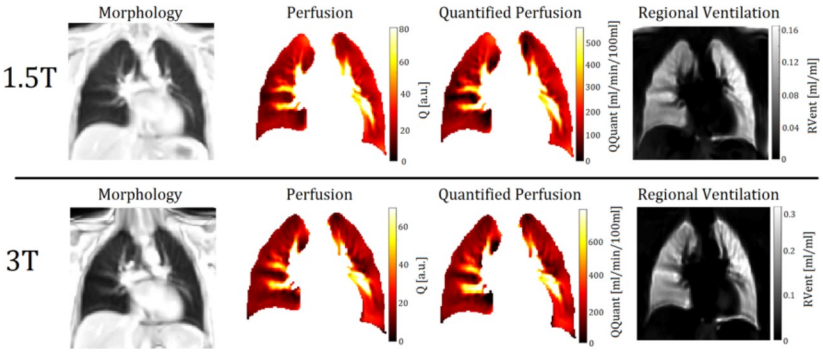

Fig 3. Exemplary PREFUL derived perfusion- and ventilation-weighted maps of a 30-year-old female participant at 1.5T and 3T. Notice the differing scaling.

https://doi.org/10.1371/journal.pone.0244638.g003

calculated by taking the difference between the signal at the time with the highest and the lowest signal of the perfusion weighted time series in the segmented parenchyma ROI. Perfusion quantification (Q_{Quant}) in ml/min/100ml was calculated by normalizing the signal of every voxel to the signal of a completely blood-filled voxel (S_{Blood}) according to Kjørstad et al. [30]:

$$Q_{Quant} = \frac{Q}{S_{Blood}} * \frac{1}{2 * t_{perf}} \quad (2)$$

Q represents the perfusion calculated as described above, S_{Blood} represents the corresponding amplitude of the aorta signal (completely blood-filled voxel) and t_{perf} represents the time between two heartbeats. Perfusion- and quantified perfusion-weighted maps generated at 1.5T and 3T are displayed in Fig 3.

Perfusion and ventilation maps

Perfusion defect percentage maps (QDP maps), ventilation defect percentage maps (VDP maps) and ventilation/perfusion match maps (VQ maps) between each corresponding 1.5T and 3T series were calculated. The upper thresholds for voxels labeled as defect were the median value– 1.75 * standard deviation (SD) for RVent and the median value– 0.75 * standard deviation for Q similarly to Voskrebenzev et al. [12]. The thresholds were set to maintain a VDP $< 10\%$ and a QDP $< 20\%$ for healthy participants.

SNR and CNR

Considering the non-central chi distribution in magnitude images of multi-channel receive coils, the SNR was estimated from the ratio of the mean signal in a ROI of the lung parenchyma and the mean signal in a ROI of the background of the image [31]. CNR was calculated by subtraction of the SNR of the parenchyma from the SNR of a lung vessel. Both parameters were calculated for the expiratory and inspiratory phase of each subject at similar ROI positions.

Statistics

The statistical analysis was performed using JMP Pro 13 (SAS Institute, Cary, NC) and MATLAB R2018a (The MathWorks, Natick, MA). Pretesting with the Shapiro-Wilk test revealed no normal distribution for all parameters. Hence, significant differences of the functional parameters (RVent, Q, Q_{Quant}, QDP, VDP and VQ-match percentages) between both corresponding series were assessed by the non-parametric Wilcoxon signed-rank test. Sørensen–Dice coefficients depicting the spatial overlap of QDP und VDP between both series were calculated. Additionally, skewness and kurtosis of the Q- and RVent-values (Fig 4) and the R^2-fit of the Q-values to the sine function were calculated for both series. Results with $P < 0.05$ were considered as significant. A retrospective sample size calculation and power calculation for three-day repeatability based on the calculated Bland-Altman plots of QDP, VDP, VQM and Q_{Quant} were performed. The calculations are based on a paired t-test using the standard deviations of the mean differences and the mean differences or the number of subjects. The level of significance was set to $\alpha \leq 0.05$ and the power level (1-β) to ≥ 0.80.

Results

Patient characteristics

The participants included 5 females and 10 males within an age range of 23 years to 55 years and a mean age of 33 years without active smokers. The height ranged from 167 cm to 192 cm

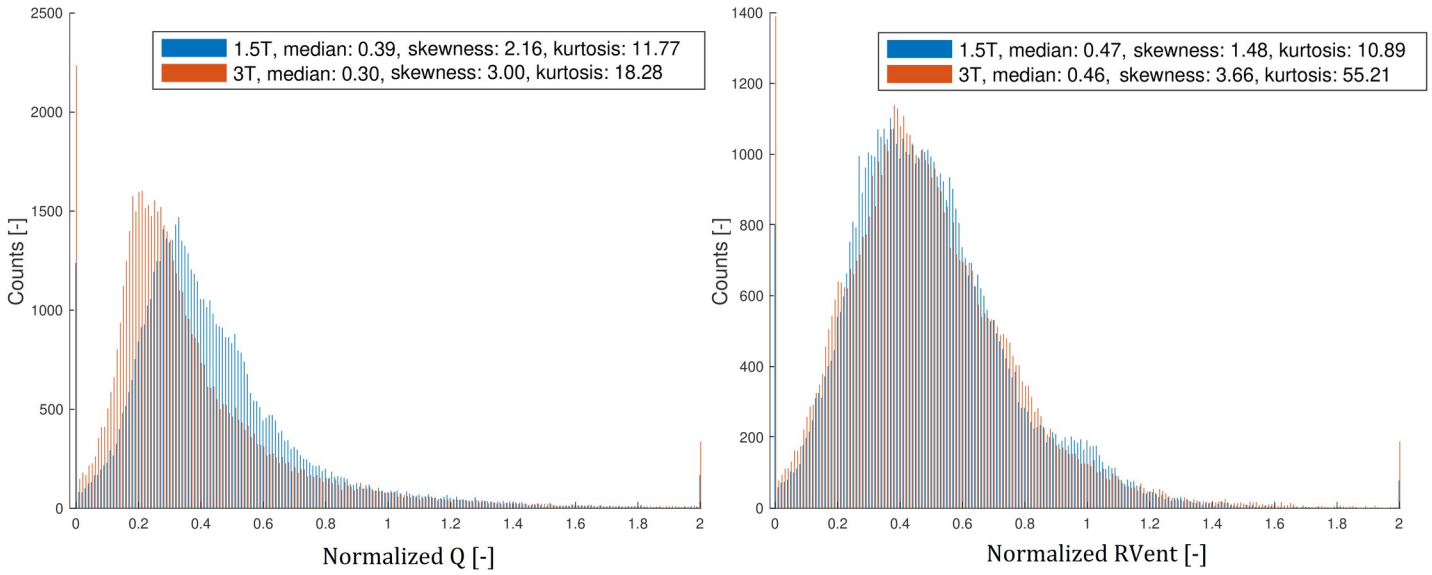

Fig 4. Histogram analysis of the normalized Q- and RVent- values of all participants. The Q- and RVent-values were normalized by division by the 95th percentile of each distribution.

https://doi.org/10.1371/journal.pone.0244638.g004

with a mean height of 178 cm. The weight ranged from 58 kg to 85 kg with a mean weight of 72 kg. The BMI ranged from 17.96 to 28.06 with a mean value of 22.82.

Functional parameters, histogram analysis and SNR/CNR

Co-registration was successful for all participants with a mean structural similarity index (SSIM) value of 52.52. The median functional parameters of both series are presented in Table 2. No significant changes were observed for RVent, Q and VDP. On the other hand, Q_{Quant} (339 ml/min/100 ml vs. 246 ml/min/100 ml) and QDP (8.15% vs. 5.04%) decreased significantly at 3T. According to the decrease of QDP and VDP, the VQM increased significantly at 3T (88.78% vs. 91.82%).

Table 3 discloses a significant increase of the median skewness (1.94 vs. 2.53) and kurtosis (8.31 vs. 11.42) of the Q-values at 3T. Fig 4 displays the increasing skewness and kurtosis of the Q- and RVent-values of all participants one histogram analysis.

Table 2. Functional parameters of all participants.

	Functional parameters			Wilcoxon signed-rank test
	1.5 Tesla	3 Tesla	Difference	*P*-value
RVent (ml/ml)	0.14 (0.10;0.16)	0.18 (0.14;0.27)	+ 0.04 (+ 29%)	0.06
Q (a.u.)	21.97 (16.95;27.16)	18.39 (15.54;20.61)	- 3.58 (- 16%)	0.21
Q_{Quant} (ml/min/100 ml)	339 (212;457)	246 (197;311)	- 93 (- 27%)	0.03*
QDP (%)	8.15 (7.09;11.34)	5.04 (3.16;6.99)	- 3.11 (- 38%)	≤0.01*
VDP (%)	4.39 (2.70;6.91)	3.36 (0.26;5.54)	- 1.03 (- 23%)	0.21
VQM (%)	88.78 (84.02;89.20)	91.82 (91.01;94.03)	- 3.04 (- 3.4%)	≤0.01*

Values are displayed as median with the first and third quartile (Q1;Q3). Significant results are marked with *.

RVent: Regional ventilation; Q: Perfusion; Q_{Quant}: Quantified perfusion; QDP: Perfusion defect percentage; VDP: Ventilation defect percentage; VQM: Ventilation perfusion match

https://doi.org/10.1371/journal.pone.0244638.t002

Table 3. Skewness and kurtosis of Q and RVent of all participants.

	Skewness and kurtosis of Q and RVent			Wilcoxon signed-rank test
	1.5 Tesla	3 Tesla	Difference	*P*-value
Skewness Q	1.94 (1.44;2.12)	2.53 (2.12;2.82)	+ 0.59 (+ 30%)	≤0.01*
Kurtosis Q	8.31 (6.87;10.53)	11.42 (9.24;15.25)	+ 3.11 (+ 37%)	≤0.01*
Skewness V	0.02 (-0.21;0.65)	0.38 (0.06;1.86)	+ 0.36 (+ 1800%)	0.08
Kurtosis V	4.00 (2.88;5.88)	5.46 (2.77;17.64)	+ 1.46 (+ 37%)	0.41

Values are displayed as median with the first and third quartile (Q1;Q3). Significant results are marked with *.

https://doi.org/10.1371/journal.pone.0244638.t003

As demonstrated in Table 4, neither the CNR nor the SNR increased significantly at 3T.

Bland-Altman analysis

The mean differences were 4.29% for QDP, 1.23% for VDP, -5.15% for VQM and 54 ml/min/100ml for Q_{Quant} in the Bland-Altman analysis (see Fig 5). A minimal sample size of 12 subjects is necessary to detect significant differences in QDP and VQM according to our retrospective sample size calculation.

Sørensen-Dice and VQ-maps

The mean Sørensen-Dice coefficients depicting the spatial overlap between both series were 0.91 for QDP, 0.94 for VDP and 0.87 for VQM using the above-mentioned thresholds. Median values of the binary maps QDP and VDP are displayed in Table 2.

Discussion

The first main finding of our study is, that neither the parameters RVent, Q and VDP, nor the SNR or the CNR altered significantly at 3T. Despite marked absolute and relative differences of the functional parameters, no significance was shown. As presented in Table 4, significance is not directly dependent on relative or absolute differences, but rather on the value distribution and standard deviation respectively. The median SNR during the expiratory state ranges between 1.5T and 3T from 10.01 to 8.47, which is in good agreement with previous reports of Yu et al. [32]. Also, the up to 95% increase of CNR was not significant. The higher field strength and advanced hardware of the 3T scanner were used to increase the temporal resolution by minimizing TR and TE rather than to improve SNR and CNR.

The second main finding of our study is the significant 27% decrease of Q_{Quant} at 3T. In a previous study, the opposite effect was shown after the administration of gadolinium based contrast agents [19]. As a well-known effect of higher field strengths is an increase of T1

Table 4. SNR and CNR results of all participants.

	Signal and Contrast to Noise Ratio			Wilcoxon signed-rank test
	1.5 Tesla	3 Tesla	Difference	*P*-value
SNR Expiration	10.01 (7.22;12.30)	8.47 (7.53;10.74)	- 1.54 (- 15%)	0.74
SNR Inspiration	7.33 (5.63;9.02)	6.56 (5.11;8.00)	- 0.77 (- 11%)	0.48
CNR Expiration	7.96 (7.10;14.66)	15.55 (8.99;21.65)	+ 7.59 (+ 95%)	0.23
CNR Inspiration	7.86 (6.39;14.76)	13.12 (9.03;18.98)	+ 5.26 (+ 67%)	0.14

Values are displayed as median with the first and third quartile (Q1;Q3).

https://doi.org/10.1371/journal.pone.0244638.t004

relaxation time of blood in the lungs, it is not surprising to see correspondingly lower values for Q_{Quant} in this study [21, 33].

The third main finding of our study is the significant 38% decrease of QDP at 3T, although we were using the same relative thresholds based on the median and the standard deviation. Significant increases of the skewness and the kurtosis confirmed our assumption of a different distribution of the Q-values at 3T (Fig 4). The mean R^2 of the piecewise fits of the Q-values to the sine function decreased not significantly from 0.55 at 1.5T to 0.45 at 3T ($P = 0.11$). Nevertheless, there is high spatial agreement between the QDP maps and also between the VDP maps of 1.5T and 3T with Sørensen-Dice coefficients of > 0.9 with the used thresholds. This is because differing nuances of the value distribution between 1.5T and 3T are not considered in binary maps like QDP and VDP and because there were very few defect areas in healthy participants at the used thresholds.

According to the before mentioned increase of T1, $T2^*$ decreases more than T2 due to higher field inhomogeneities, susceptibility effects and spin-spin interactions [20, 34, 35]. Again, this could be a potential cause for the differing distributions of the Q- and RVent-values–expressed by significant increases of the skewness and the kurtosis–at 3T.

Beside the earlier mentioned characteristics of lung tissue with low intrinsic signal and high susceptibility artifacts, the two-compartment model of extravascular lung water (EVLW) and intravascular lung water (IVLW) in the human lung could be a possible explanation for different signal alteration of Q-maps and RVent-maps at higher field strengths. Triphan et al. explain, that T1 is not only highly variable, but also, that both compartments of the lung tissue contain different values of T1 and $T2^*$. Assuming a relatively slow proton exchange compared to the relaxation times of the compartments, long TEs are predominantly measuring intravascular protons, whereas short TEs are measuring the extravascular compartment [36]. Likewise, the variability of $T2^*$ between subjects is very high [37], but may be negligible during tidal breathing [32]. Bydder et al. point out that all tissues have multicomponent T2s resulting of a mixture of different T2 components [38]. In this regard, it is important to understand the non-linear relationship between relaxation rate and field strength [32, 39]. This would explain a differing sensibility of perfusion- and ventilation-maps on field strength, as their signal is based on intravascular flow related enhancement (Q-map) or combined intra- and extravascular lung density changes (RVent-map).

Possible improvements at higher field strengths could be achieved by the use of modified imaging sequences in regards to the SAR limits, artifacts and field inhomogeneities, the image contrast and higher SNR [39]. Rotärmel et al. already demonstrated the advantages of steady-state free precession (SSFP) over the GRE Fast Low Angle Shot (FLASH) sequence regarding SNR and lung-vessel-contrast at 1.5T [40].

In this context the results of Bauman et al. are very promising. Whereas a balanced steady-state free precession (bSSFP) sequence is sensitive to artifacts and endangers SAR limits by using high flip angles, the proposed transient spoiled gradient echo (tSPGR) acquisitions provided a significant increase in SNR to contemporary spoiled gradient recalled (SPGR) acquisitions at 3T [24].

The main limitation of our study is the difference of the used sequence parameters–flip angle, TE and TR–between 1.5T and 3T. The respective functionality of the sequences at 1.5T and 3T is given, but any modification of the sequence would entail a reevaluation of the functional parameters to guarantee comparability. For instance a smaller flip angle of 4˚ was used at 3T to compensate for the increasing T1 of blood at 3T [41]. Additionally, the advanced hardware with differing coil design of the 3T Skyra allows for higher slew rates of up to 200 mT/m/ms leading to higher imaging speed and temporal resolution.

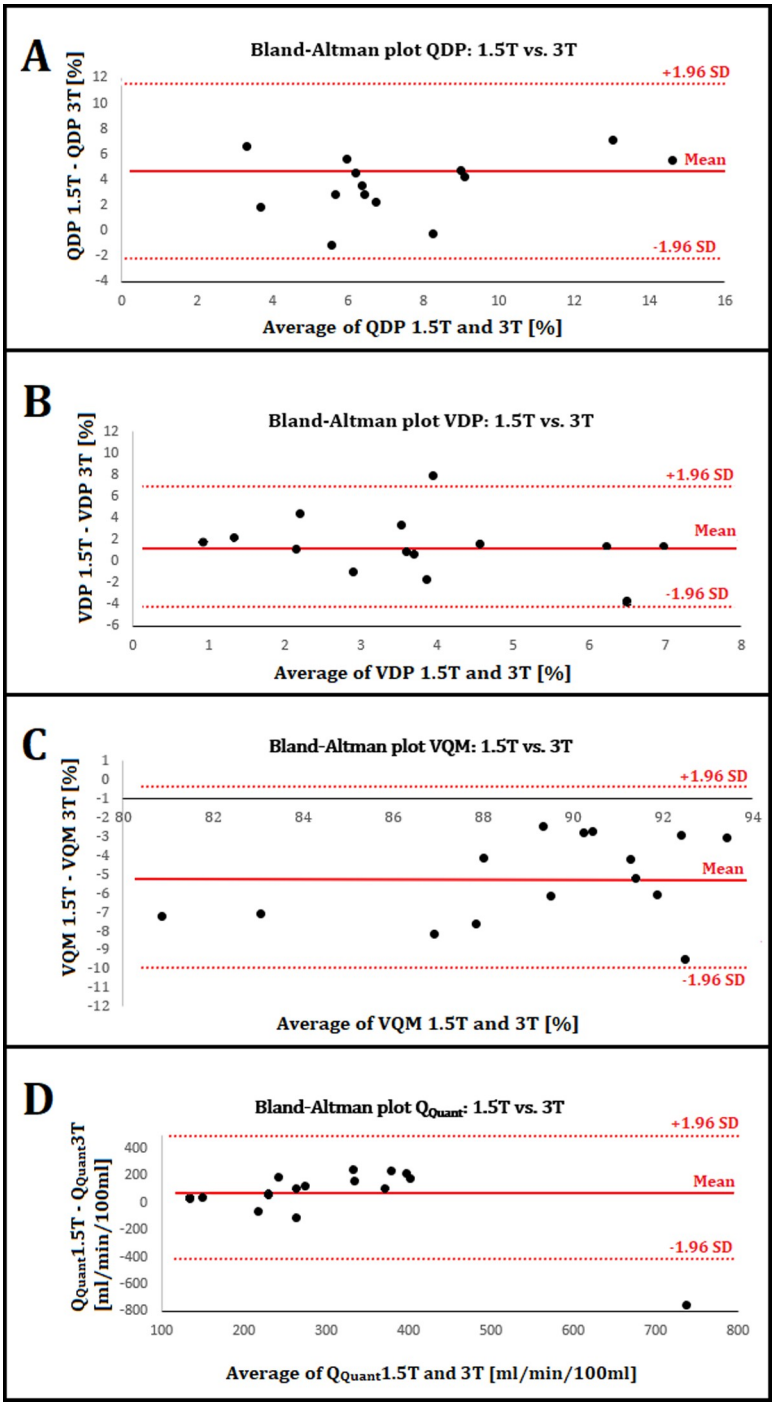

Fig 5. Bland-Altman plots. A) The mean average of QDP ((QDP 1.5T –QDP 3T)/2) is 7.39% and the mean difference (QDP 1.5T –QDP 3T) (solid red lines) is 4.29% with a SD of 3.54%. The upper and lower 95% confidence intervals mean ± 1.96*SD (dashed red lines) are 11.23% and -2.64%. **B)** The mean average of VDP is 4.04% and the mean difference is 1.23% with a SD of 2.76%. The confidence intervals are 6.64% and -4.18%. **C)** The mean average of VQM is 89.44% and the mean difference is -5.15% with a SD of 2.45%. The confidence intervals are -0.35% and -9.95%. **D)** The mean average of Q_{Quant} is 314 ml/min/100ml and the mean difference is 54 ml/min/100ml with a SD of 246 ml/min/100ml. The confidence intervals are 537 and -428 ml/min/100ml.

https://doi.org/10.1371/journal.pone.0244638.g005

A further limitation of our study is the lack of more established reference standards such as 129-Xe ventilation MRI and dynamic contrast enhanced perfusion MRI as gold standards [42, 43]. By having a group of healthy participants, it is very difficult to set a comprehensive threshold for QDP and VDP. Although these parameters have proven to be highly valuable in various studies with patients [12, 17, 44], there is limited interstudy comparability, because their thresholds were set differently according to the underlying data. As healthy participants only have rare perfusion and ventilation defect areas, it is not surprising to achieve Dice-values of over 0.9. Additionally, FD derived functional parameters have shown to exhibit good, but still limited reproducibility [19, 45, 46]. In particular perfusion quantification is influenced by various technical and physiological circumstances, like field inhomogeneities, physiological breathing and perfusion variability, inaccuracy of the estimated receive coil sensitivities or the angle of blood flow towards the imaging plane [47]. For example, no randomization of the 1.5T and 3T scanner was done. By this, participants could have been more relaxed during the second scan already knowing the procedure.

Beside RVent and Q_{Quant}, more fully quantified functional parameters need to be developed in further studies to achieve optimal comparability and their dependency on varying relaxation times needs to be considered. Ideally, a multicompartment mapping of PD, T1 and T2 would be helpful, but has not been developed or published yet. The functional parameters could potentially be adapted to these tissue characteristics.

Conclusion

RVent, Q, VDP, SNR and CNR were not altered significantly at the used parameters. Significant differences in QDP may be related to the field strength. Q_{Quant} reveals only poor reproducibility between 1.5T and 3T. Healthy participants with minimal defects present high spatial agreement of QDP and VDP.

Supporting information

S1 Dataset. Dataset of all results.
(XLSX)

Acknowledgments

The authors would like to express their thanks to the medical technical assistants Frank Schröder and Melanie Pfeifer from the Department of Radiology for their support in the MR measurements and patient care.

Author Contributions

Conceptualization: Jens Vogel-Claussen.

Formal analysis: Julian Glandorf, Filip Klimeš, Andreas Voskrebenzev.

Funding acquisition: Jens Vogel-Claussen.

Investigation: Julian Glandorf.

Methodology: Julian Glandorf, Marcel Gutberlet.

Project administration: Frank Wacker, Jens Vogel-Claussen.

Resources: Frank Wacker, Jens Vogel-Claussen.

Software: Filip Klimeš, Andreas Voskrebenzev, Marcel Gutberlet, Lea Behrendt.

Supervision: Frank Wacker, Jim M. Wild, Jens Vogel-Claussen.

Writing – original draft: Julian Glandorf.

Writing – review & editing: Julian Glandorf, Filip Klimeš, Andreas Voskrebenzev, Marcel Gutberlet, Lea Behrendt, Cristian Crisosto, Frank Wacker, Pierluigi Ciet, Jim M. Wild, Jens Vogel-Claussen.

References

1. Forum of International Respiratory Societies. The Global Impact of Respiratory Disease—Second Edition. Sheffield; 2017.
2. World Health Organization. World health statistics 2008. Geneva; 2008.
3. Ebert M, Grossmann T, Heil W, et al. Nuclear magnetic resonance imaging with hyperpolarised helium-3. Lancet 1996; 347:1297–1299 https://doi.org/10.1016/s0140-6736(96)90940-x PMID: 8622506
4. Kauczor H-U. Hyperpolarized helium-3 gas magnetic resonance imaging of the lung. Top. Magn. Reson. Imaging 2003; 14:223–30.
5. Couch MJ, Ball IK, Li T, Fox MS, Biman B, Albert MS. 19 F MRI of the Lungs Using Inert Fluorinated Gases: Challenges and New Developments. J. Magn. Reson. Imaging 2019; 49:343–354 https://doi.org/10.1002/jmri.26292 PMID: 30248212
6. Hopkins SR, Wielpütz MO, Kauczor HU. Imaging lung perfusion. J. Appl. Physiol. 2012; 113:328–339 https://doi.org/10.1152/japplphysiol.00320.2012 PMID: 22604884
7. Cha MJ, Kang DY, Lee W, et al. Hypersensitivity Reactions to Iodinated Contrast Media: A Multicenter Study of 196 081 Patients. Radiology 2019; 293:117–124 https://doi.org/10.1148/radiol.2019190485 PMID: 31478801
8. Grobner T. Gadolinium—A specific trigger for the development of nephrogenic fibrosing dermopathy and nephrogenic systemic fibrosis? Nephrol. Dial. Transplant. 2006; 21:1104–1108 https://doi.org/10.1093/ndt/gfk062 PMID: 16431890
9. Enright PL, Beck KC, Sherrill DL. Repeatability of Spirometry in 18,000 Adult Patients. Am. J. Respir. Crit. Care Med. 2004; 169:235–238 https://doi.org/10.1164/rccm.200204-347OC PMID: 14604836
10. Zapke M, Topf HG, Zenker M, et al. Magnetic resonance lung function—A breakthrough for lung imaging and functional assessment? A phantom study and clinical trial. Respir. Res. 2006; 7:106 https://doi.org/10.1186/1465-9921-7-106 PMID: 16889671
11. Bankier AA, O'Donnell CR, Mai VM, et al. Impact of lung volume on MR signal intensity changes of the lung parenchyma. J. Magn. Reson. Imaging 2004; 20:961–966 https://doi.org/10.1002/jmri.20198 PMID: 15558552
12. Voskrebenzev A, Gutberlet M, Klimeš F, et al. Feasibility of quantitative regional ventilation and perfusion mapping with phase-resolved functional lung (PREFUL) MRI in healthy volunteers and COPD, CTEPH, and CF patients. Magn. Reson. Med. 2017; 79:2306–2314 https://doi.org/10.1002/mrm.26893 PMID: 28856715
13. Kaireit TF, Gutberlet M, Voskrebenzev A, et al. Comparison of quantitative regional ventilation-weighted fourier decomposition MRI with dynamic fluorinated gas washout MRI and lung function testing in COPD patients. J. Magn. Reson. Imaging 2018; 47:1534–1541 https://doi.org/10.1002/jmri.25902 PMID: 29160020
14. Voskrebenzev A, Greer M, Gutberlet M, et al. Detection of chronic lung allograft dysfunction using ventilation-weighted Fourier decomposition MRI. Am. J. Transplant. 2018; 18:2050–2060 https://doi.org/10.1111/ajt.14759 PMID: 29607606
15. Schoenfeld C, Cebotari S, Hinrichs J, et al. MR Imaging–derived Regional Pulmonary Parenchymal Perfusion and Cardiac Function for Monitoring Patients with Chronic Thromboembolic Pulmonary Hypertension before and after Pulmonary Endarterectomy. Radiology 2016; 279:925–934 https://doi.org/10.1148/radiol.2015150765 PMID: 26727392
16. Veldhoen S, Weng AM, Knapp J, et al. Self-gated Non–Contrast-enhanced Functional Lung MR Imaging for Quantitative Ventilation Assessment in Patients with Cystic Fibrosis. Radiology 2017; 283:242–251 https://doi.org/10.1148/radiol.2016160355 PMID: 27715657
17. Vogel-Claussen J, Schönfeld CO, Kaireit TF, et al. Effect of indacaterol/glycopyrronium on pulmonary perfusion and ventilation in hyperinflated patients with chronic obstructive pulmonary disease (CLAIM) a double-blind, randomized, crossover trial. Am. J. Respir. Crit. Care Med. 2019; 199:1086–1096 https://doi.org/10.1164/rccm.201805-0995OC PMID: 30641027

18. Klimeš F, Voskrebenzev A, Gutberlet M, et al. Free-breathing quantification of regional ventilation derived by phase-resolved functional lung (PREFUL) MRI. NMR Biomed. 2019; 32:e4088 https://doi.org/10.1002/nbm.4088 PMID: 30908743

19. Glandorf J, Klimeš F, Voskrebenzev A, Gutberlet M, Wacker F, Vogel-Claussen J. Effect of intravenously injected gadolinium-based contrast agents on functional lung parameters derived by PREFUL MRI. Magn. Reson. Med. 2019:1–10 https://doi.org/10.1002/mrm.27991 PMID: 31517406

20. Soher BJ, Dale BM, Merkle EM. A Review of MR Physics: 3T versus 1.5T. Magn. Reson. Imaging Clin. N. Am. 2007; 15:277–290 https://doi.org/10.1016/j.mric.2007.06.002 PMID: 17893049

21. Barth MM, Smith MP, Pedrosa I, Lenkinski RE, Rofsky NM. Body MR imaging at 3.0 T: Understanding the opportunities and challenges. Radiographics 2007; 27:1445–1462 https://doi.org/10.1148/rg.275065204 PMID: 17848702

22. Kauczor H-U, Kreitner K-F. Contrast-enhanced MRI of the lung. Eur. J. Radiol. 2000; 34:196–207 https://doi.org/10.1016/s0720-048x(00)00199-6 PMID: 10927161

23. Mulkern R, Haker S, Mamata H, et al. Lung parenchymal signal intensity in MRI: A technical review with educational aspirations regarding reversible versus irreversible transverse relaxation effects in common pulse sequences. Concepts Magn. Reson. Part A Bridg. Educ. Res. 2014; 43:29–53 https://doi.org/10.1002/cmr.a.21297 PMID: 25228852

24. Bauman G, Pusterla O, Bieri O. Functional lung imaging with transient spoiled gradient echo. Magn. Reson. Med. 2019; 81:1915–1923 https://doi.org/10.1002/mrm.27535 PMID: 30346077

25. Avants BB, Tustison NJ, Song G, Cook PA, Klein A, Gee JC. A reproducible evaluation of ANTs similarity metric performance in brain image registration. Neuroimage 2011; 54:2033–2044 https://doi.org/10.1016/j.neuroimage.2010.09.025 PMID: 20851191

26. Voskrebenzev A, Gutberlet M, Kaireit TF, Wacker F, Vogel-Claussen J. Low-pass imaging of dynamic acquisitions (LIDA) with a group-oriented registration (GOREG) for proton MR imaging of lung ventilation. Magn. Reson. Med. 2017; 78:1496–1505 https://doi.org/10.1002/mrm.26526 PMID: 27859552

27. Wang Z, Bovik AC, Sheikh HR, Simoncelli EP. Image quality assessment: From error visibility to structural similarity. IEEE Trans. Image Process. 2004; 13:600–612 https://doi.org/10.1109/tip.2003.819861 PMID: 15376593

28. He K, Sun J, Tang X. Guided image filtering. IEEE Trans. Pattern Anal. Mach. Intell. 2013; 35:1397–1409 https://doi.org/10.1109/TPAMI.2012.213 PMID: 23599054

29. Klimeš F, Voskrebenzev A, Gutberlet M, et al. Free-breathing quantification of regional ventilation derived by phase-resolved functional lung (PREFUL) MRI. NMR Biomed. 2019:e4088 https://doi.org/10.1002/nbm.4088 PMID: 30908743

30. Kjørstad Å, Corteville DMR, Fischer A, et al. Quantitative lung perfusion evaluation using fourier decomposition perfusion MRI. Magn. Reson. Med. 2014; 72:558–562 https://doi.org/10.1002/mrm.24930 PMID: 24006024

31. Constantinides CD, Atalar E, McVeigh ER. Signal-to-noise measurements in magnitude images from NMR phased arrays. Magn. Reson. Med. 1997; 38:852–857 https://doi.org/10.1002/mrm.1910380524 PMID: 9358462

32. Yu J, Xue Y, Song HK. Comparison of lung T2* during free-breathing at 1.5 T and 3.0 T with ultrashort echo time imaging. Magn. Reson. Med. 2011; 66:248–254 https://doi.org/10.1002/mrm.22829 PMID: 21695727

33. Stanisz GJ, Odrobina EE, Pun J, et al. T1, T2 relaxation and magnetization transfer in tissue at 3T. Magn. Reson. Med. 2005; 54:507–512 https://doi.org/10.1002/mrm.20605 PMID: 16086319

34. Hatabu H, Alsop DC, Listerud J, Bonnet M, Gefter WB. T2* and proton density measurement of normal human lung parenchyma using submillisecond echo time gradient echo magnetic resonance imaging. Eur. J. Radiol. 1999; 29:245–252 https://doi.org/10.1016/s0720-048x(98)00169-7 PMID: 10399610

35. Gai ND, Malayeri AA, Bluemke DA. Three-dimensional T1 and T2* mapping of human lung parenchyma using interleaved saturation recovery with dual echo ultrashort echo time imaging (ITSR-DUTE). J. Magn. Reson. Imaging 2017; 45:1097–1104 https://doi.org/10.1002/jmri.25487 PMID: 27726231

36. Triphan SMF, Jobst BJ, Breuer FA, et al. Echo time dependence of observed T1 in the human lung. J. Magn. Reson. Imaging 2015; 42:610–616 https://doi.org/10.1002/jmri.24840 PMID: 25604043

37. Theilmann RJ, Arai TJ, Samiee A, et al. Quantitative MRI measurement of lung density must account for the change in T2 * with lung inflation. J. Magn. Reson. Imaging 2009; 30:527–534 https://doi.org/10.1002/jmri.21866 PMID: 19630079

38. Bydder GM. The Agfa Mayneord lecture: MRI of short and ultrashort T2and T2* components of tissues, fluids and materials using clinical systems. Br. J. Radiol. 2011; 84:1067–1082 https://doi.org/10.1259/bjr/74368403 PMID: 22101579

39. Bottomley PA, Foster TH, Argersinger RE, Pfeifer LM. A review of normal tissue hydrogen NMR relaxation times and relaxation mechanisms from 1–100 MHz: Dependence on tissue type, NMR frequency, temperature, species, excision, and age. Med. Phys. 1984; 11:425–448 https://doi.org/10.1118/1.595535 PMID: 6482839

40. Rotärmel A, Voskrebenzev A, Klimes F, Gutberlet M, Wacker F, Vogel- J. GRE bSSFP vs. FLASH based Fourier Decomposition lung MRI at 1.5T: evaluation of image quality, fractional ventilation and lung perfusion in healthy volunteers. Proc. Intl. Soc. Mag. Reson. Med. 26 2018:2–4 https://doi.org/10.1002/nbm.3134.8

41. Zhang X, Petersen ET, Ghariq E, et al. In vivo blood T1 measurements at 1.5 T, 3 T, and 7 T. Magn. Reson. Med. 2013; 70:1082–1086 https://doi.org/10.1002/mrm.24550 PMID: 23172845

42. Kern AL, Biller H, Klimeš F, et al. Noninvasive Monitoring of the Response of Human Lungs to Low-Dose Lipopolysaccharide Inhalation Challenge Using MRI: A Feasibility Study. J. Magn. Reson. Imaging 2019:jmri.27000 https://doi.org/10.1002/jmri.27000 PMID: 31729119

43. Sourbron S, Ingrisch M, Siefert A, Reiser M, Herrmann K. Quantification of cerebral blood flow, cerebral blood volume, and blood-brain-barrier leakage with DCE-MRI. Magn. Reson. Med. 2009; 62:205–217 https://doi.org/10.1002/mrm.22005 PMID: 19449435

44. Guo F, Capaldi DPI, McCormack DG, Fenster A, Parraga G. A framework for Fourier-decomposition free-breathing pulmonary 1 H MRI ventilation measurements. Magn. Reson. Med. 2019; 81:2135–2146 https://doi.org/10.1002/mrm.27527 PMID: 30362609

45. Lederlin M, Bauman G, Eichinger M, et al. Functional MRI using Fourier decomposition of lung signal: Reproducibility of ventilation- and perfusion-weighted imaging in healthy volunteers. Eur. J. Radiol. 2013; 82:1015–1022 https://doi.org/10.1016/j.ejrad.2012.12.003 PMID: 23295084

46. Voskrebenzev A, Gutberlet M, Becker L, Wacker F, Vogel-Claussen J. Reproducibility of fractional ventilation derived by Fourier decomposition after adjusting for tidal volume with and without an MRI compatible spirometer. Magn. Reson. Med. 2016; 76:1542–1550 https://doi.org/10.1002/mrm.26047 PMID: 26745750

47. Behrendt L, Voskrebenzev A, Klimeš F, et al. Validation of Automated Perfusion-Weighted Phase-Resolved Functional Lung (PREFUL)-MRI in Patients With Pulmonary Diseases. J. Magn. Reson. Imaging 2019:jmri.27027 https://doi.org/10.1002/jmri.27027 PMID: 31872556